Mineralogical Magazine, April 1999, Vol. 63(2), pp. 149–163

Defect structure and luminescence behaviour of agate — results of electron paramagnetic resonance (EPR) and cathodoluminescence (CL) studies

J. GÖTZE[1], M. PLÖTZE[1], H. FUCHS[1] AND D. HABERMANN[2]

[1] Department of Mineralogy, Freiberg University of Mining and Technology, D-09596 Freiberg, Germany
[2] Department of Geology, Ruhr-University Bochum, D-44780 Bochum, Germany

ABSTRACT

Samples of agate and quartz incrustations from different parent volcanic rocks of certain world-wide localities were investigated by EPR, CL and trace element analysis. In all agate samples the following paramagnetic centres were detected: O_2^{3-}, E'_1, $[AlO_4]^0$, $[FeO_4/M^+]^0$, and $[GeO_4/M^+]^0$. Centres of the type $[TiO_4/Li^+]^0$ and $[TiO_4/H^+]^0$, which were detected in quartz of the parent volcanics, are absent in agate. Generally, the abundance of O_2^{3-} centres (silicon vacancy) and E'_1 centres (oxygen vacancy) in agate is remarkably higher than in quartz. The high defect density in agates points to rapid growth of silica from a strongly supersaturated solution probably with a noncrystalline precursor.

CL microscopy reveals internal structures and zoning in agates and quartz incrustations which clearly differ from those discernible by conventional polarizing microscopy. The CL spectra of agates differ from those of quartz from crystalline rocks. At least three broad emission bands were detected in the CL spectra: a blue band of low intensity, a yellow band at about 580 nm, and an intense red band at 650 nm. The CL emission at 650 nm shows some relations to the hydroxyl or alkali content and the abundance of O_2^{3-} centres and E'_1 centres. The emission intensity increases during electron bombardement due to the conversion of different precursors (e.g. ≡Si-O-H, ≡Si-O-Na groups) into hole centres. Another conspicuous feature in the CL spectra of agates is the existence of a yellow emission band centred at around 580 nm. The predominance of the yellow CL emission band and the high concentration of E'_1 centres are typical for agates of acidic volcanics and are indicative of a close relationship between the two.

KEYWORDS: quartz, agate, electron paramagnetic resonance, cathodoluminescence, trace elements, defect structure.

Introduction

SiO_2 (silica) makes up 12.6 wt.% of the Earth's crust as crystalline and noncrystalline silica in 14 modifications (Strunz and Tennyson, 1982). The most common modification is the trigonal low-temperature quartz (α-quartz) which occurs extensively in various geological environments. One of the most conspicuous forms of microcrystalline α-quartz is agate (banded chalcedony), which is sometimes formed as cavity infillings especially in volcanic rocks. Despite world wide agate occurrences and numerous investigations, the process of formation of agate is not yet completely understood. An advanced classification of microcrystalline quartz is established in accordance with compositional and structural characteristics (cf. Flörke *et al.*, 1991; Graetsch, 1994) showing certain structural disparities between chalcedony and macrocrystalline quartz (e.g. Heany *et al.*, 1994). In contrast to the intensively studied quartz, much less is known about point defects in agates and the luminescence behaviour, which is mainly controlled by trace element impurities and lattice defects.

In the present study, the application of advanced analytical methods such as EPR, CL, and trace element analyses (INAA, AES) should provide more information concerning the real structure of agate and genetic aspects of agate

formation. The aim of this study was to evaluate similarities and differences in the abundance and distribution of paramagnetic defects between macrocrystalline quartz and agate samples from various locations and different parent rocks, respectively. Moreover, relations between the real structure and the luminescence behaviour of agate should be revealed.

Materials and methods

In the present study agates of certain volcanic rocks were investigated (see Table 2). The analysed material includes samples from 18 localities world-wide, of different age (Precambrian to Tertiary), and of different parent rocks (acidic, intermediate, and basic volcanic parent rocks).

The sample material was carefully crushed and agate (partially separated coloured bands) and quartz incrustations were separated from the parent rock material by hand-picking under a binocular microscope. The separated fractions were treated with distilled water to remove adhering particles and then air dried. Representative aliquots of the samples were analysed for trace element contents by instrumental neutron activation analysis (INAA — see Götze and Lewis, 1994) and atomic emission spectroscopy (AES) according to Schrön *et al.* (1983), respectively.

The paramagnetic centres of natural as well as irradiated (^{60}Co, 295 K, 2100 Gy and 10^6 Gy for Al centre saturation, respectively) agate and quartz samples were investigated by EPR at frequencies of the X-band (9.5 GHz) at 20, 70, and 295 K. Before γ-irradiation the samples were heated at 400°C for 5 h to anneal the paramagnetic centres formed by natural irradiation. Spectra were recorded by a Varian E-line spectrometer. The sample temperature was controlled with a low temperature unit based on a helium gas flow device (Oxford ESR 900A). The influence of technical parameters such as modulation amplitude, microwave power, temperature, scan time etc. on the spectra were checked for the optimal settings for recording the spectra. These settings (modulation field H_M = 1 G, temperature T = 295 K, microwave power p = 0.2 mW for E′ and 30 mW for oxygen-associated hole centres (O^-) and H_M = 1 G, p = 7 mW, T = 70 K for $[AlO_4]^0$ centres) were kept constant throughout all the measurements to allow correct comparison between the signal intensities of different spectra. The concentration of the paramagnetic centres was determined as peak to peak or peak to base intensity at the analytical lines (Moiseev,, 1985). The specific peak positions of the paramagnetic centres were drawn from simulated spectra and from data from the literature. The program of Nettar and Villafranca (1985) was used for the powder spectra simulations. The variation of intensity detected by repeated measurements of selected analytical lines is up to 10%. The concentration of Al centres was quantified using a reference sample with known $[AlO_4]^0$ concentration (Moiseev, 1985). All other centres were calculated in relative amounts.

Cathodoluminescence examinations were carried out on polished thin-sections using a 'hot cathode' CL microscope. The system was operated at 14 kV and with a current density of about 10 μA/mm^2. Thin-sections were coated with carbon to prevent any build-up of electrical charge during CL operation. Coloured photomicrographs were taken using Kodak Ektachrome 400 HC. CL spectra were obtained using an EG&G digital triple-grating spectrograph with CCD detector. The CCD camera was attached to the CL microscope by a silica-glass fibre-guide (cf. Neuser *et al.*, 1995). Cathodoluminescence spectra were measured in the wavelength range 320 to 800 nm using standardized conditions (accumulation time 10 s, spot width 30 μm). To prevent any falsification of the CL spectra due to electron bombardment, all spectra were taken on samples that were not irradiated by an electron beam before analysis.

Results and discussion

EPR measurements

The results of EPR analyses in this study represent first systematic investigations concerning the defect structure of agates. The analyses provide information on the abundance and distribution of paramagnetic lattice defects and trace elements which are incorporated and produce a paramagnetic centre in the quartz structure. The paramagnetic centres were classified according to Table 1.

Generally, agate shows a different distribution of centres from quartz of crystalline rocks (Götze and Plötze, 1997). In all agate samples the following paramagnetic centres were detected: O_2^{3-}, E'_1, $[AlO_4]^0$, $[FeO_4/M^+]^0$, and $[GeO_4/M^+]^0$ (Table 2). The occurrence of Mn^{2+} centres is

TABLE 1. Common paramagnetic centres in quartz (after Plötze, 1995)

		Foreign ion centres		Vacancies	
		Si^{4+} substitution	Interstitial	Oxygen vacancies	Silicon vacancies
Metastable	Electron centres ($+ e^-$)	$[TiO_4]^-$ $[TiO_4/M^+]^0$ $[GeO_4]^-$ $[GeO_4/M^+]^0$		*E′* centres: $[SiO_3]^{3-}$	
	Defect electron centres ($- e^-$)	$[AlO_4]^0$ $[FeO_4]^0$			*O^- centres*: O^-, O_2^{3-}, O_2^{3-}-M^+
Stable (paramagnetic without charge receive)		$[FeO_4/M^+]^0$? $[FeO_4]^-$ (precursor for $[FeO_4]^0$	Fe^{3+}		

M^+ = interstitial H^+, Li^+, Na^+

attributed to the presence of calcite microinclusions and is not assumed to be incorporated into the quartz lattice. Centres of the type $[TiO_4/Li^+]^0$ and $[TiO_4/H^+]^0$, which were detected in quartz of the parent volcanic rocks, are absent in agate indicating different conditions of formation. These $[TiO_4^-/M^+]^0$ centres are produced by irradiation of the diamagnetic precursor $[TiO_4]^0$ (Ti^{3+}; i.e. electron centre at Ti^{4+}) which is formed by substitution of Ti^{4+} for Si^{4+} at the Si position, where charge compensation is achieved by a proton or Li^+ ion at a channel position nearby (Wright *et al.*, 1963; Rinneberg and Weil, 1972) (Fig. 1).

The $[SiO_3]^{3-}$ centre (E'_1 centre) consists of an unpaired electron bound on a O^{2-} vacancy (e.g. Weeks, 1956; Weil, 1984). The O^- and O_2^{3-} centres represent different types of defect electrons on O^{2-} in tetrahedra with silicon vacancy (e.g. Bershov *et al.*, 1978; Serebrennikov *et al.*, 1982) (Fig. 2).

Generally, the abundance of O_2^{3-} centres (silicon vacancy) and E'_1 centres (oxygen vacancy) in agate is noticeably high. This high defect density in agates points to rapid growth of silica from a strongly supersaturated solution probably with a noncrystalline precursor (e.g. rapid cooling). This assumption is emphasized by the comparison of the centre concentration in agate with that in the quartz incrustations (Table 2; Fig. 3). The quartz crystals within agate geodes show lower concentrations of O_2^{3-} and E'_1 centres indicating slower crystallization from a mother fluid without supersaturation. Furthermore, a differentiation of agates from acidic and basic parent rocks is possible using the concentration of O_2^{3-} and E'_1 centres (Fig. 3). The high concentration of vacancy centres in agates (especially of acidic volcanics) can be related to the conversion of non-paramagnetic precursors into paramagnetic centres by self-irradiation due to the high contents of U and other radioactive elements. The results of trace element analyses show U concentrations of up to 21.4 ppm (Table 2). Figure 4 shows a slight correlation between U content and the concentration of E'_1 centres in agates especially in those with U concentrations >5 ppm.

Another group of paramagnetic centres is connected with substitutional and interstitial trace element incorporation into the quartz lattice. In the investigated agate and quartz samples $[AlO_4]^0$, $[FeO_4/M^+]^0$, and $[GeO_4/M^+]^0$ centres were detected.

The $[AlO_4]^0$ centre (Fig. 1) is caused by substitution of Al^{3+} for Si^{4+} with an electron hole at one of the four nearest O^{2-} ions, forming O^{1-} (Griffiths *et al.*, 1954). The precursor state for this centre is the diamagnetic $[AlO_4/M^+]^0$ associated with an adjacent charge compensating cation M^+ (H^+, Li^+, Na^+). Results of Heany and Davis (1995) indicate the predominance of Na^+ as charge compensating cation in agate. During γ-irradiation of quartz at 295 K, the M^+-ion may

TABLE 2. Results of EPR measurements and analysis of selected trace elements

No. Location	Sample	Al [ppm]	$[AlO_4]^\circ$ [1E+16 spin/g]	Fe [ppm]	Fe^{3+} arb. units	$[GeO_4/M^+]^\circ$ arb. units	O_2^{3-} arb. units	E'_1 arb. units	U [ppm]
Nova Paka. Bohemia (rhyolite)									
1–4	agate. white	>1200	78.7	891	39.0	15.5	100.0	27.0	1.2
1–5	agate. grey	>1200	88.0	2060	10.8	13.5	85.5	24.0	1.1
1–6	agate. grey	>1200	97.2	2720	15.4	13.5	80.5	21.3	1.1
1–7	agate. red	>1200	88.0	1150	3.8	–	94.0	34.8	3.3
Idar-Oberstein. Germany (andesite)									
3–3	agate. white	277	61.7	697	3.8	8.5	120.0	65.0	11.0
3–4	agate. red	606	154.3	770	105.0	–	147.5	67.5	18.7
Lauterbach. Germany (rhyolite)									
6–6	agate. white	>1200	54.0	370	3.5	–	120.0	44.8	6.1
6–7	agate. red	>1200	69.5	594	5.0	–	152.5	107.5	21.1
6–8	agate. dark	>1200	69.5	312	5.0	–	87.5	53.5	9.6
6–10	quartz	>1200	25.9	1150	3.4	–	2.3	2.5	0.3
6–11	amethyst	135	31.6	647	3.1	1.4	3.3	3.5	0.4
Frydstejn. Bohemia (melaphyre)									
17–2	agate. white	359	94.1	220	2.4	10.0	54.0	3.8	0.1
17–3	agate. red	314	57.1	279	3.4	–	70.0	3.3	<0.1
17–4	agate. white	543	135.8	83	3.6	–	119.5	4.3	n.d.
Rio Grande do Sul. Brazil (basalt)									
18–2	agate	114	126.6	84	3.5	10.0	29.5	1.0	4.3
Kyje. Bohemia (rhyolite)									
19–2	agate	104	63.3	33	9.6	–	86.0	48.8	n.d.
19–3	agate. brown	144	71.0	433	11.6	–	11.5	39.8	n.d.
19–4	agate. red	202	68.7	1340	11.6	–	90.0	23.0	n.d.
Ardownie Quarry. Scotland (andesite)									
20–2	agate	266	172.9	27	3.1	–	40.0	2.3	0.1
20–3	quartz	162	19.7	37	3.0	1.1	4.1	2.3	0.1
Montrose. Scotland (andesite)									
22–2	agate. white	456	101.1	69	2.8	–	92.0	3.5	<0.1
22–3	agate. red	>1200	123.5	119	7.5	–	71.0	3.0	0.1
22–5	quartz	109	40.7	130	2.3	1.8	3.1	1.8	n.d.
Chihuahua. Mexico (andesite)									
24–3	agate	172	37.8	12	3.1	–	60.5	5.8	21.3
24–4	agate. yellow	998	50.9	136	5.0	–	58.0	6.3	16.1
24–5	quartz	n.d.	13.1	n.d.	3.1	3.8	5.0	3.6	4.2
Agate Point. Canada (basalt)									
40–2	agate	392	78.7	92	3.8	–	55.0	16.0	0.7
40–3	agate. red	445	66.4	561	2.9	–	42.5	17.8	0.6
40–6	quartz	n.d.	45.9	n.d.	3.0	1.8	5.9	2.4	0.2
Otter Cove. Canada (basalt)									
41–2	agate. white	412	84.9	112	3.1	–	50.3	3.5	n.d.
41–3	agate. red	626	81.8	206	2.9	–	40.0	3.3	n.d.
41–4	quartz	n.d.	24.7	n.d.	2.8	2.1	2.5	1.8	n.d.
Agate Island. Canada (basalt)									
42–2	agate. white	170	54.0	234	3.6	–	30.0	2.3	n.d.
42–3	agate. red	164	27.0	433	2.6	–	12.5	1.3	n.d.

TABLE 2. (*contd.*)

No. Location	Sample	Al [ppm]	$[AlO_4]^0$ [1E+16 spin/g]	Fe [ppm]	Fe^{3+} arb. units	$[GeO_4/M^+]^0$ arb. units	O_2^{3-} arb. units	E'_1 arb. units	U [ppm]
Agate Island. Canada (basalt)									
43–2	agate. white	154	72.5	478	2.9	–	35.0	1.8	2.9
43–3	agate. red	264	97.2	418	3.3	–	41.5	2.3	3.9
43–4	quartz	101	38.8	85	2.4	1.6	5.9	2.1	1.5
Callenberg. Germany (altered basic wall rock)									
45–2	agate. white	99	43.7	118	5.9	2.8	23.6	3.1	2.2
45–3	agate. black	791	17.7	3630	24.3	–	16.0	5.5	2.9
Halsbach. Germany (vein agate)									
46–1	agate. white	>1200	169.8	389	6.3	6.8	35.8	3.0	0.6
46–2	agate. red	348	71.0	1950	4.9	8.5	92.0	3.6	14.9
46–3	quartz	106	26.2	125	3.1	–	3.8	3.8	0.4
Schlottwitz. Germany (vein agate)									
47–3	quartz	182	7.5	153	2.6	1.0	3.0	1.5	2.9
Gröppendorf. Germany (melaphyre)									
48–1	agate	>1200	169.8	636	7.8	1.4	10.8	2.6	3.9
48–8	quartz I	348	71.0	647	3.6	–	4.1	1.9	5.1
48–9	quartz II	106	26.2	863	2.5	–	1.3	1.8	2.2
Sarusa Mine. Namibia (andesite)									
51–1	quartz	79	8.9	8.3	3.4	0.8	1.8	0.9	<0.1
51–2	agate	>1200	118.8	404	74.0	41.3	187.5	7.4	0.2

n.d.: not determined; (–): below detection limit

diffuse away yielding the paramagnetic $[AlO_4]^0$ (Nuttall and Weil, 1981). Irradiation experiments in the present study confirm earlier results (Plötze *et al.*, 1998) in which an irradiation dose of about 10^6 Gy causes a complete conversion of nonparamagnetic Al-precursors into the paramagnetic $[AlO_4]^0$ centres.

The concentration of the Al centres was quantified using a reference sample with known $[AlO_4]^0$ concentration (Moiseev, 1985). A comparison of the concentration of structurally incorporated Al with the content of bulk trace Al was now possible (10^{16} spin/g Al = 1 ppm Al). The results in Table 2 show that the concentration of bulk 'trace element Al' is higher than structural 'EPR Al'. Nevertheless, the comparison reveals that a considerable amount of the trace Al is indeed incorporated into the quartz structure and not only within microinclusions.

Some Fe^{3+} paramagnetic centres can occur in quartz. One of these centres is characterized by substitution of Fe^{3+} for Si^{4+} with charge compensation by alkali ions or protons, so-called *S* centres $[FeO_4/M^+]^0$ (Stegger and Lehmann, 1989; Mineeva *et al.*, 1991). The broad line by $g_{eff} \approx 4.3$ is characteristic of substitutional Fe^{3+} centres in quartz. The comparison of the Fe^{3+}-centre concentration with Fe contents analysed by AES shows that there is no correlation and that only some of the iron is incorporated in the quartz structure. Even red chalcedony bands often show relatively low concentrations of substitutional Fe indicating that the colour is caused by fine dispersed iron oxides.

Substitution of Si^{4+} by Ge^{4+} causes the formation of the diamagnetic precursor $[GeO_4]^0$ which transforms to the paramagnetic $[GeO_4]^-$ during γ-irradiation. At room temperature these centres can bound diffusing M^+ cations preferentially forming $[GeO_4/Li^+]^0$ and $[GeO_4/H^+]^0$ (Mackey, 1963; Rakov *et al.*, 1985; Weil, 1993). $[GeO_4/M^+]^0$ centres were detected after irradiation in some of the samples only in quartz

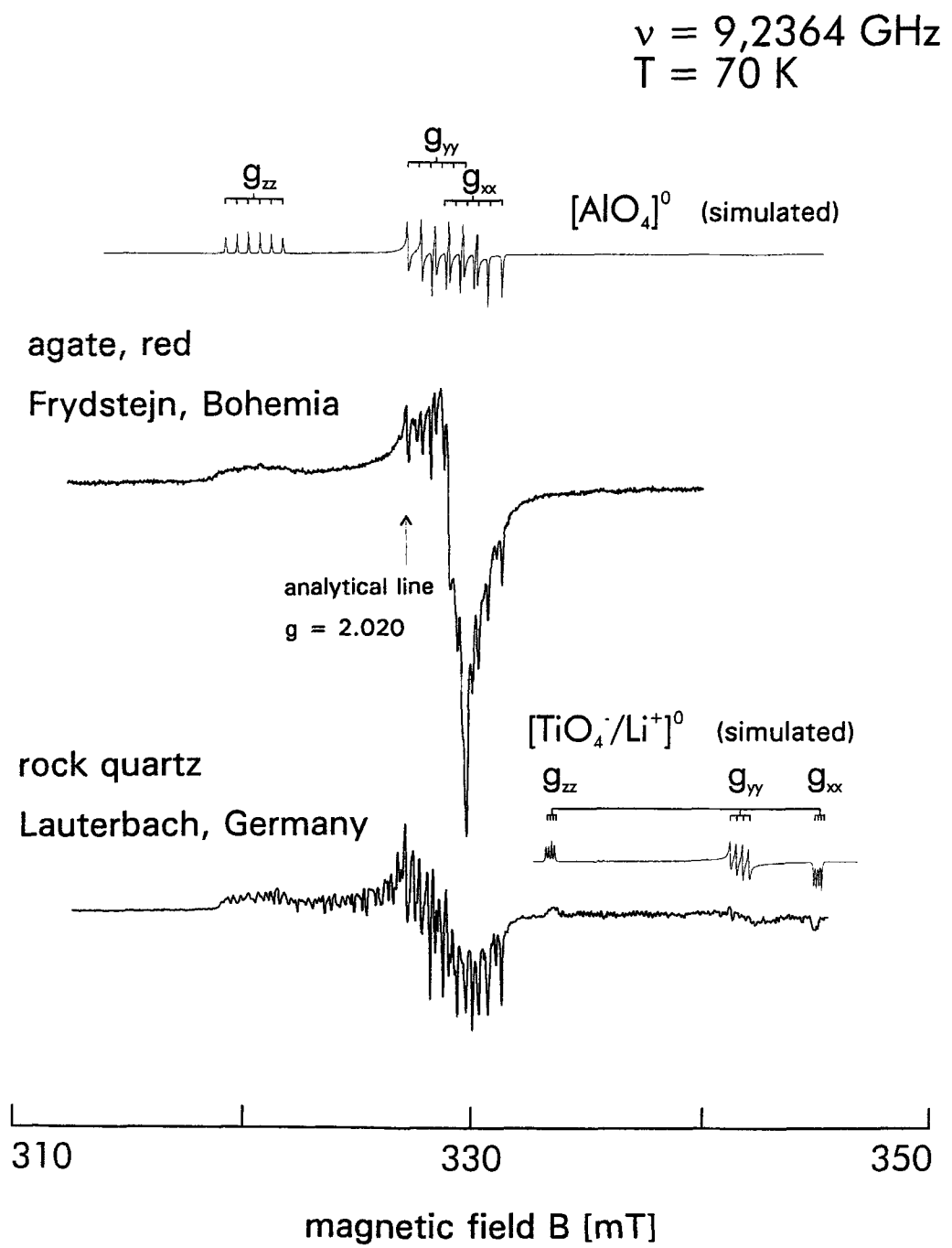

FIG. 1. Selected EPR spectra of trace element centres the investigated samples in comparison with simulated spectra (arrows mark analytical lines).

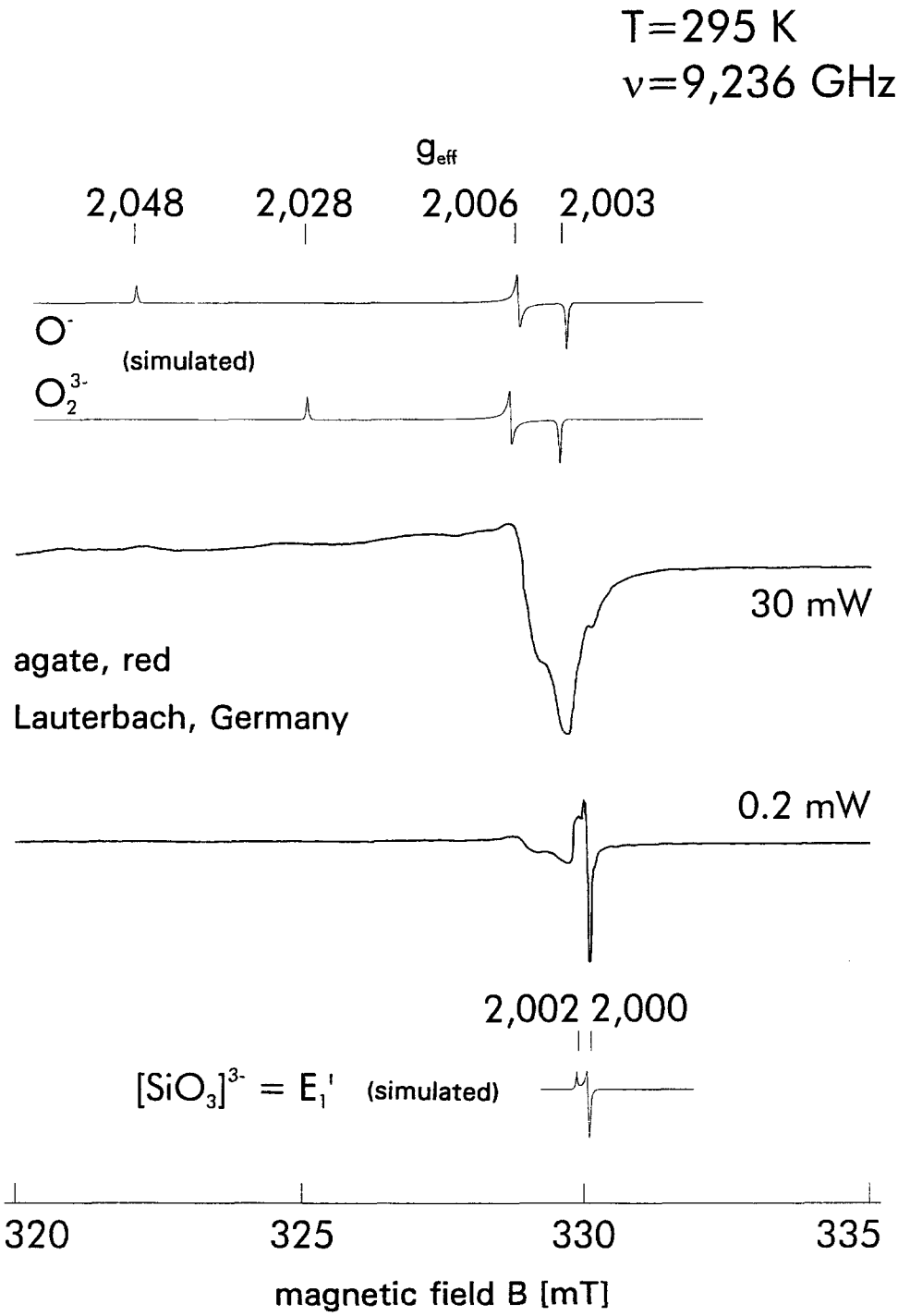

FIG. 2. Simulated EPR spectra (O^-, O_2^{3-}, E'_1) in comparison with detected spectra in the agate samples investigated (analytical lines are marked by arrows).

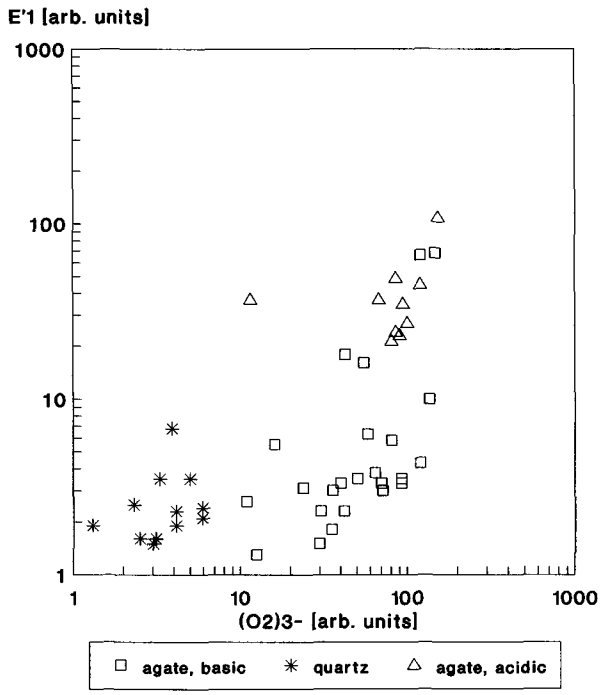

FIG. 3. Abundance of O_2^{3-} and E'_1 centres in agates and quartz incrustations of the investigated samples. Agates of basic and acidic volcanics and associated quartz incrustations are clearly distinguishable by their defect density.

incrustations of agate geodes. This result corresponds with conclusions of Blankenburg (1988) who found high concentrations of Ge (up to 30 ppm) in quartz incrustations rather than in the agates.

Cathodoluminescence

Based on the available results of CL studies of all samples a remarkable differentiation of agates of basic and acidic volcanics is possible in respect to their luminescence behaviour. Furthermore, structural characteristics of agates and corresponding quartz incrustations can be revealed due to varying luminescence behaviour.

Agates and quartz incrustations of acidic volcanics exhibit multi-coloured, predominantly stable luminescence with colours of yellow, red, pink and blue (Plate 1). Earlier investigations (Götze, 1996) have shown that CL spectra of the agates are more complex than those of phanerocrystalline rock quartz. This is caused by high concentrations of intrinsic lattice defects and several trace elements which are incorporated into the structure and act as luminescence centres. Veinlike agates in acid volcanics also show a long-lived, multi-coloured luminescence (Plate 2).

In basic volcanics both agates and quartz incrustations exhibit short-lived blue cathodoluminescence. The intensity of the blue luminescence colour falls off rapidly within the range of 30 to 60 seconds of electron bombardement. The resulting luminescence colours are different shades of reddish brown (Plate 3). This CL behaviour is similar to that reported by Ramseyer *et al.* (1988) especially for fracture fillings or idiomorphic vein crystals of hydrothermal origin. Ramseyer *et al.* (1988) reported short-lived bottle-green or blue CL colours in alpha quartz which they related to the presence of Al and interstitial charge compensating cations of Li and Na (conversion of $[AlO_4/M^+]^0$ to $[AlO_4]^0$ + diffusing M^0).

Structural characteristics of agates and corresponding quartz incrustations could be revealed

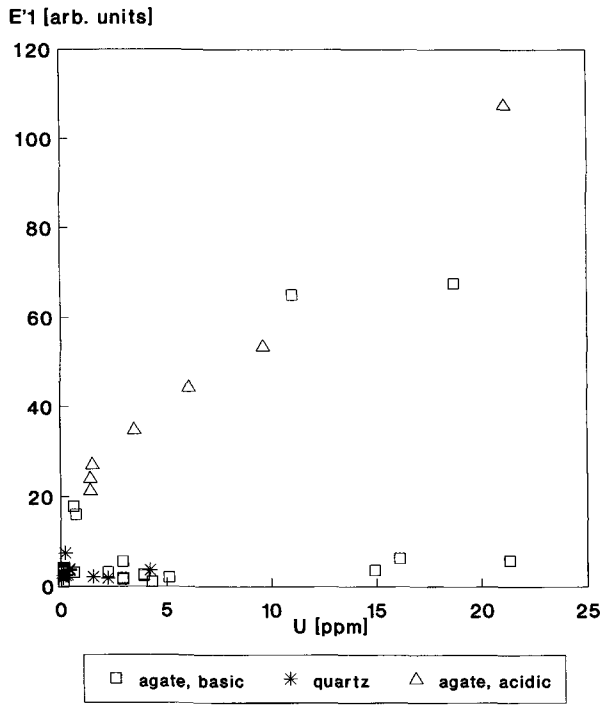

FIG. 4. Correlation of U content versus concentration of E'_1 centres of the investigated samples.

by CL. Agates commonly show concentric zoning under CL. In most quartz crystals CL reveals distinct zoning and internal structures remarkably differing from those visible under crossed polars (Plate 4). Often quartz crystals consist of fragments, which show partial zoning. Some of these structural defects, which are not common in ideal quartz, may be interpreted as stranded structural states that are residual from rapid crystal growth.

More detailed information about the CL behaviour is provided by spectral measurements. Agates of various origin show different CL behaviour and the CL spectra of agates differ from those of quartz. At least three broad emission bands were detected in the CL spectra: a blue band of low intensity, a band at about 580 nm, and an intense red band at 650 nm (Figs. 5–8). The CL colours observed are caused by varying intensity ratios of these CL emission bands and indicate variations of lattice defects in zones with different CL colour.

The blue CL emission band, which usually dominates in the CL spectra of quartz, is weak or absent in the CL spectra of agates (Figs. 5–8). According to Gorton *et al.* (1996) this luminescence band consists of overlapping component bands of different polarisation and quenching temperatures. Gorton *et al.* (1996) used a phase-tuning technique to separate and identify the lines from different centres. They found four major components of the blue cathodoluminescence emission band at 390 nm, 420 nm, 450 nm, and 500 nm in almost all investigated synthetic and natural quartzes.

A transient blue emission (380–390 nm) was especially observed under the CL microscope in agates of basic volcanics. This emission is very sensitive to irradiation damage and was found to correlate well with the Al content and the concentration of $[AlO_4/M^+]^0$ centres (Alonso *et al.*, 1983; Luff and Townsend, 1990; Perny *et al.*, 1992; Gorton *et al.*, 1996). Therefore, this emission has been attributed to the trapping of a hole to that substitutional, charge-compensated aluminium-alkali ion centre (Stevens Kalceff and Phillips, 1995). The rapid attenuation of the 390 nm emission under an electron beam results from the conversion of all $[AlO_4/M^+]^0$ to the paramagnetic

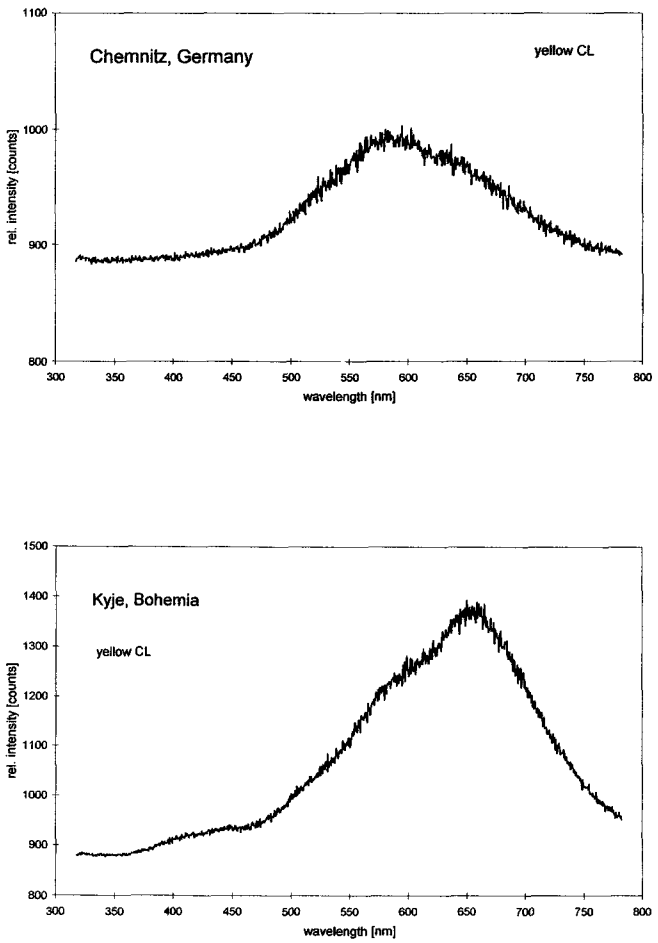

FIG. 5. Cathodoluminescence spectra of agates from acidic volcanics dominated by the yellow emission band at 580 nm and the red band at 650 nm.

$[AlO_4]^0$ centre and the dissociation and electromigration of the charge compensating cations out of the interaction volume under the influence of the irradiation induced electrical field. This short-lived CL can be restored by heating the quartz up to 500°C for one day (Perny *et al.*, 1992) indicating an opposite mechanism to that of TL. Although the transient blue emission in agates was visible under the CL microscope, the optical characteristic of the used fibre glass and the specific detector sensitivity prevent the detailed spectral characterisation of this emission band. Therefore, a correlation between the intensity of the short-lived blue emission and the concentration of Al centres could not be established.

The red emission band at *c.* 650 nm has been detected in almost all agates and quartz incrustations as the most intense emission in the CL spectrum. This emission is attributed to the recombination of electrons in the non-bridging oxygen band-gap state with holes in the valence-band edge (Siegel and Marrone, 1981). A number of different precursors of this non-bridging oxygen hole centre have been proposed such as hydrogen or sodium impurities ($\equiv$Si-O-H, $\equiv$Si-O-Na groups), peroxy linkages (oxygen-rich samples), or strained silicon-oxygen bonds (Stevens Kalceff and Phillips, 1995). Upon irradiation impurity atoms diffuse away and form non-bridging oxygen centres (e.g. O^-,

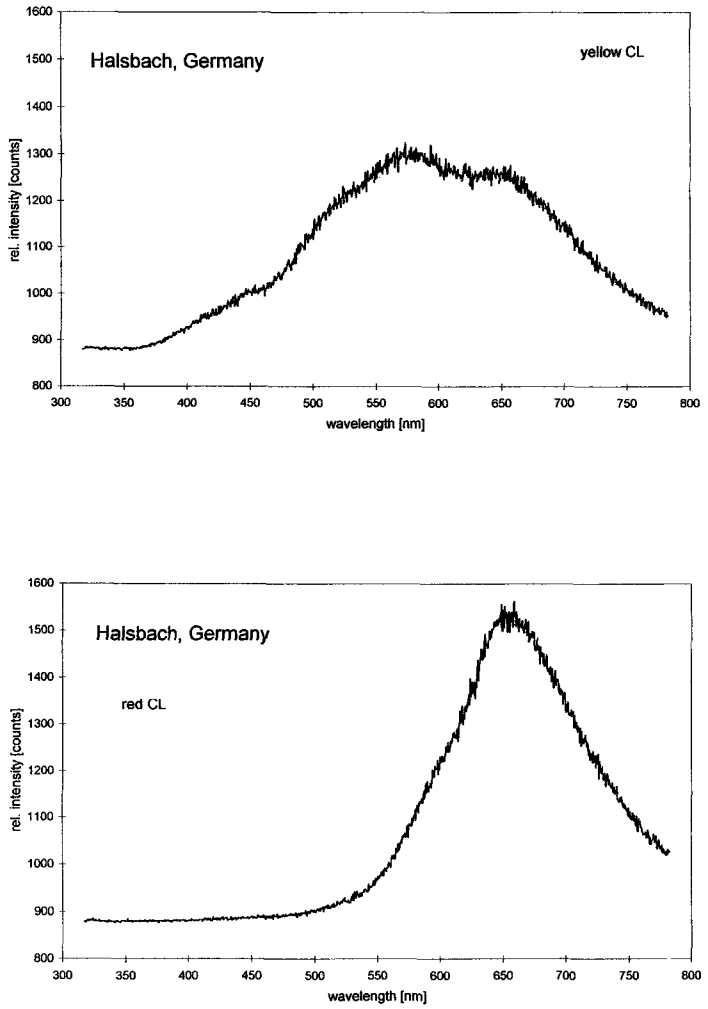

FIG. 6. Cathodoluminescence spectra of differently luminescing zones within the veinlike agate from Halsbach, Germany showing quite different emission bands.

O_2^{3-}). Therefore, the CL emission at 1.9 eV (650 nm) increases initially during electron bombardement and then stabilizes (Fig. 8). We conclude that high intensities of the 650 nm emission in agate can probably be assigned to high concentration of O_2^{3-} centres (comp. Table 2) which are formed by irradiation (natural and electron bombardement). Silanol groups ($\equiv$Si-O-H), which are a constituent of the agate structure (Flörke *et al.*, 1982), are the favourable precursors of these non-bridging oxygen centres in agates.

Another conspicuous feature in the CL spectra of agates is the existence of a yellow emission band centred on 580 nm. This CL emission is especially dominant in agates of acidic volcanics (Figs. 5,6). An emission band at 560 to 580 nm was first observed by Rink *et al.* (1993) in TL spectra of natural quartz of hydrothermal origin and was interpreted by these authors as related to oxygen vacancies. Correspondingly, Fuchs and Götze (1996) found this yellow CL emission in agates and hydrothermal vein quartz showing high contents of intrinsic defects and Si-substituting

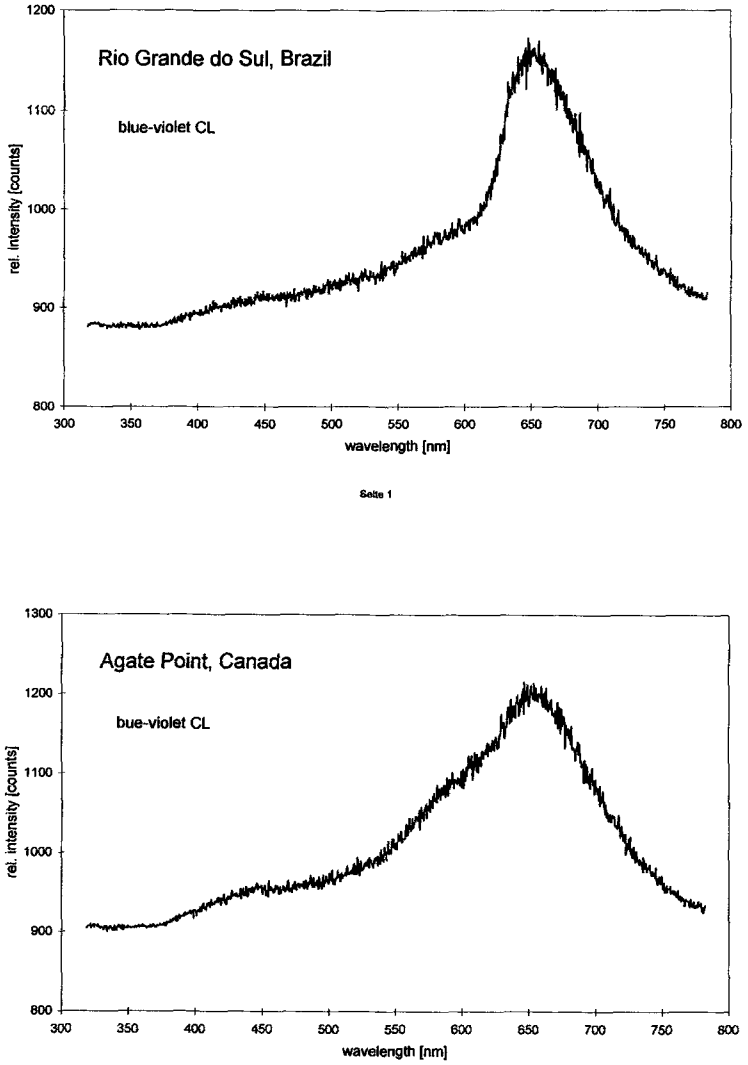

FIG. 7. Cathodoluminescence spectra of agates from basic volcanics showing a dominant red emission band at 650 nm. The short-lived emission band around 380 nm was not detectable due to the low detector efficiency in this wavelength range.

elements. The predominance of the yellow CL emission band and the high concentration of E'_1 centres were found to be typical for agates of acidic volcanics which indicates a close relationship.

Conclusions

The real structure of agates and quartz incrustations from certain occurrences was investigated by EPR and CL measurements. The agates and corresponding quartz incrustations show varying spectroscopic behaviour.

The red emission band at *c.* 650 nm has been detected in all agates and quartz incrustations as the most intense emission in the CL spectrum. The high intensities of the 650 nm emission in agate can probably be assigned to high concentration of O_2^{3-} centres. The EPR measurements show for the agates extremely high concentrations of this centre. Silanol groups ($\equiv$Si-O-H) are the

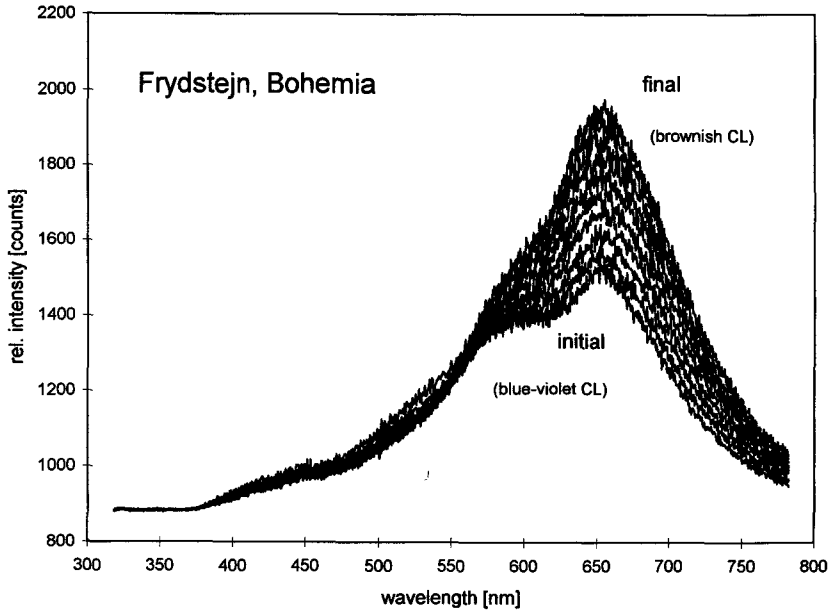

FIG. 8. Time dependent cathodoluminescence spectra of agate from Frydland, Bohemia; the time-scan (10 × 5 s) illustrates the strong intensity increase of the 650 nm emission during electron bombardement.

favourable precursors of these non-bridging oxygen centres in agates, which can be transformed into nonbridging oxygen hole centres during electron bombardement. Furthermore the results reveal remarkable differences between agates in acidic volcanics and those of basic wall rock. The transient 380–390 nm emission is especially visible in agates of basic volcanics. This emission can be attributed to the trapping of a hole to a substitutional, charge-compensated aluminium-alkali ion centre resulting in a conversion of $[AlO_4/M^+]^0$ to the paramagnetic $[AlO_4]^0$ centre. The predominance of the yellow CL emission band (580 nm) and the high concentration of E'_1 centres are both typical for agates of acidic volcanics indicating a close relationship.

The varying conditions of agate formation cause different intrinsic and extrinsic (trace element) defects in the SiO_2 structure. Generally, the abundance of intrinsic defects (silicon and oxygen vacancies, silanol groups) in agate is noticeably higher than in rock quartz. This high defect density as well as impurities in agates along with the specific textural characteristics revealed by CL point to a rapid growth of silica from a strongly supersaturated solution probably with a noncrystalline precursor. These results would confirm earlier conclusions of Heany and Davis (1995) and Götze *et al.* (1998) who showed that the agate structure can probably be interpreted as alternating formation of fine-grained, highly defective chalcedony intergrown with moganite, and coarse-grained low-defect quartz.

Acknowledgements

This research was funded by the Deutsche Forschungsgemeinschaft (DFG-grant No. GO 677/1), which we gratefully acknowledge. We thank S.S. Hafner (Marburg) who made the EPR spectrometer available for analysis of agate samples.

References

Alonso, P.J., Halliburton, L.E., Kohnke, E.E. and Bossoli, R.B. (1983) X-ray induced luminescence in crystalline SiO_2. *J. Appl. Phys.*, **54**, 5369–75.

Bershov, L.V., Krylova, M.D. and Speranskij, A.V. (1978) The electron hole centres O^--Al and Ti^{3+} as indicator for temperature conditions during regional metamorphosis (in Russ.). *Izv. Akad. Nauk SSSR,*

Ser. geol., 113–7.

Blankenburg, H.-J. (1988) *Agate* (in German). Dt. Verl. f. Grundstoffindustrie, Leipzig.

Flörke, O.W., Köhler-Herbertz, B., Langer, K. and Tönges, I. (1982) Water in microcrystalline quartz of volcanic origin: agates. *Contrib. Mineral. Petrol.*, **80**, 324–33.

Flörke, O.W., Graetsch, H., Martin, B., Röller, K. and Wirth, R. (1991) Nomenclature of micro- and non-crystalline silica minerals, based on structure and microstructure. *Neues Jahrb. Mineral., Abh.*, **163**, 19–42.

Fuchs, H. and Götze, J. (1996) Origin of volcanic agate - evidence from cathodoluminescence, EPR and geochemical studies. *Intern. Conf. CL Rel. Techn. Geosci. Geomat.*, Nancy, Abstracts, 49–50.

Gorton, N.T., Walker, G. and Burley, S.D. (1996) Experimental analysis of the composite blue CL emission in quartz — is this related to aluminium content? *Intern. Conf. CL Rel. Techn. Geosc. Geomat.*, Nancy, Abstracts 59–60.

Götze, J. (1996) Cathodoluminescence of quartz - Principle and application in geosciences (in German). *Aufschluss*, **47**, 215–23.

Götze, J. and Lewis, R. (1994) Distribution of REE and trace elements in size and mineral fractions of high purity quartz sands. *Chem. Geol.*, **114**, 43–57.

Götze, J. and Plötze, M. (1997) Investigation of trace-element distribution in detrital quartz by Electron Paramagnetic Resonance (EPR). *Eur. J. Mineral.*, **9**, 529–37.

Götze, J., Nasdala, L., Kleeberg, R. and Wenzel, M. (1998): Occurrence and distribution of 'moganite' in agate/chalcedony: A combined micro-Raman, Rietveld, and cathodoluminescence study. *Contrib. Mineral. Petrol.* (in press).

Graetsch, H. (1994) Structural characteristics of opaline and microcrystalline silica minerals. In: Silica. *Reviews in Mineralogy*, **29**, 209–32.

Griffiths, J.H.E., Owen, J. and Ward, I.M. (1954) Paramagnetic resonance in neutron-irradiated diamond and smoky quartz. *Nature*, **173**, 439–42.

Heany, P.J. and Davis, A.M. (1995) Observation and origin of self-organized textures in agates. *Science*, **269**, 1562–5.

Heany, P.J., Veblen, D.R. and Post, J.E. (1994) Structural disparities between chalcedony and macrocrystalline quartz. *Amer. Mineral.*, **79**, 452–60.

Luff, B.J. and Townsend, P.D. (1990) Cathodoluminescence of synthetic quartz.- *J. Phys. Condens. Matter*, **2**, 8089–97.

Mackey, J.H. (1963) EPR study of impurity-related color centers in germanium-doped quartz. *J. Chem. Phys.*, **39**, 74–83.

Mineeva, R.M., Bershov, L.V. and Petrov, I. (1991) EPR of surface associated Fe^{3+} in polycrystalline quartz (in Russ.). *Dokl. Akad. Nauk SSSR*, **321**, 368–72.

Moiseev, B.M. (1985) *Natural Radiation Processes in Minerals* (in Russ.). Nedra, Moscow.

Nettar, D. and Villafranca, J.J. (1985) A program for EPR powder spectren simulation. *J. Magn. Res.*, **64**, 61.

Neuser, R.D., Bruhn, F., Götze, J., Habermann, D. and Richter, D.K. (1995) Cathodoluminecence: method and application (in German). *Zbl. Geol. Paläont. Teil I*, **1/2**, 287–306.

Nuttall, R.H.D. and Weil, J.A. (1981) The magnetic properties of the oxygen-hole aluminium centers in crystalline SiO_2. I. $[AlO_4]^0$. *Canad. J. Phys.*, **59**, 1696–707.

Pearny, B., Eberhardt, P., Ramseyer, K., Mullis, J. and Pankrath, R. (1992) Microdistribution of Al, Li and Na in alpha-quartz: Possible causes and correlation with short-lived cathodoluminescence. *Amer. Mineral.*, **77**, 534–44.

Plötze, M. (1995) Investigation of quartz, scheelite and fluorite from hydrothermal rare-metal deposits by EPR (in German). *Diss. TU Bergakademie Freiberg*, 141 pp.

Plötze, M., Wolf, D. and Krbetschek, M.R. (1998) Radiation dependence of EPR and TL-spectra of quartz. *Phys. Chem. Minerals* (submitted).

Rakov, L.T., Kuvshinova, K.A., Moiseev, B.M., Pleskova, M.A. and Kandinov, M.N. (1985) Typomorphic properties of Ti centres in quartz (in Russ.). *Dokl. Akad. Nauk SSSR*, **317**, 181–5.

Ramseyer,K., Baumann, J., Matter, A. and Mullis, J. (1988) Cathodoluminescence colours of alpha-quartz. *Mineral. Mag.*, **52**, 669–77.

Rink, W.J., Rendell, H., Marseglia, E.A., Luff, B.J. and Townsend, P.D. (1993) Thermoluminescence spectra of igneous quartz and hydrothermal vein quartz. *Phys. Chem. Minerals*, **20**, 353–61.

Rinneberg, H. and Weil, J.A. (1972) EPR studies of Ti^{3+}-H^+ centers in X-irradiated alpha-quartz. *J. Chem. Phys.*, **56**, 2019–28.

Schrön, W., Kaiser, G. and Bombach, G. (1983) Trace element analysis in geological samples by emission spectrography with semiautomatic evaluation (in German). *Z. ang. Geol.*, **11**, 559–65.

Serebrennikov, A.I., Valter, A.A., Mashkovtsev, R.I. and Shcherbakova, M.Ya. (1982) The investigation of defects in shock-metamorphosed quartz. *Phys. Chem. Minerals*, **8**, 153–7.

Siegel, G.H. and Marrone, M.J. (1981) Photoluminescence in as-drawn and irradiated silica optical fibers: An assessment of the role of nonbridging oxygen defect centres. *J. Non-Cryst. Solids*, **45**, 235–47.

Stegger, P. and Lehmann, G. (1989) The structures of three centers of trivalent iron in alpha-quartz. *Phys.*

Chem. Minerals, **16**, 401–7.

Stevens Kalceff, M.A. and Phillips, M.R. (1995) Cathodoluminescence microcharacterization of the defect structure of quartz. *Phys. Rev.*, **B52**, 3122–34.

Strunz, H. and Tennyson, C. (1982) *Mineralogical Tables*. Akademie-Verl.-ges. Geest & Portig, Leipzig.

Weeks, R.A. (1956) Paramagnetic resonance of lattice defects in irradiated quartz. *J. Appl. Phys.*, **27**, 1376–81.

Weil, J.A. (1984) A review of electron spin spectroscopy and its application to the study of paramagnetic defects in crystalline quartz. *Phys. Chem. Minerals*, **10**, 149–65.

Weil, J.A. (1993) A review of the EPR spectroscopy of the point defects in α-quartz: The decade 1982–1992. In *Physics and Chemistry of SiO_2 and the Si-SiO_2 interface 2* (C.R. Helms and B.E. Deal, eds). Plenum Press, New York, 131–44.

Wright, P.M., Weil, J.A., Buch, T. and Anderson, J.H. (1963) Titanium colour centers in rose quartz. *Nature*, **197**, 246–8.

[*Manuscript received 16 September 1998*]

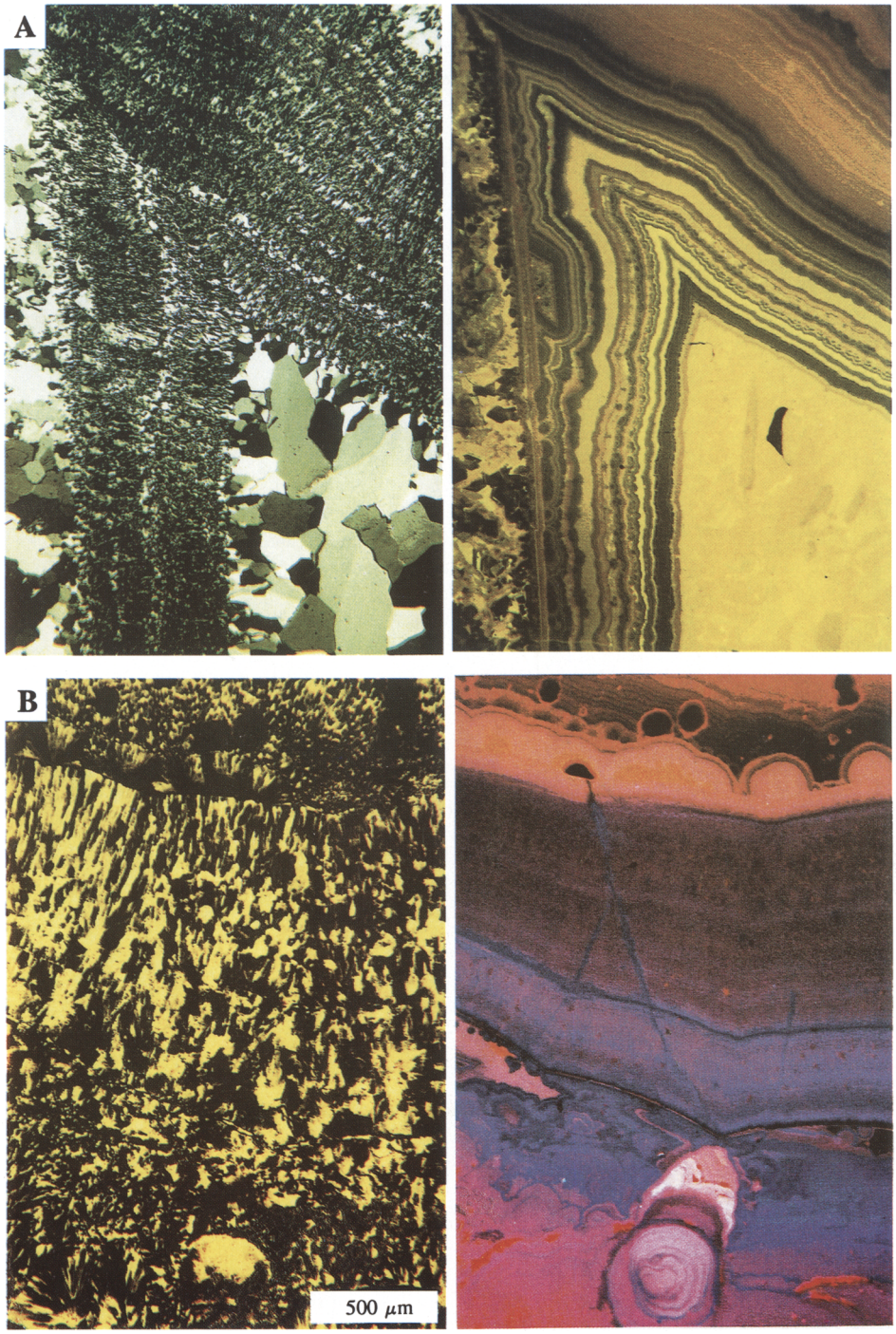

PLATE 1. Crossed polars/cathodoluminescence pairs of agates from acidic volcanics: (A) agate with associated quartz incrustation from Chemnitz, Germany showing predominantly yellow cathodoluminescence colours; (B) agate from Hohenstein-Ernstthal, Germany which exhibits multicoloured cathodoluminescence zonation.

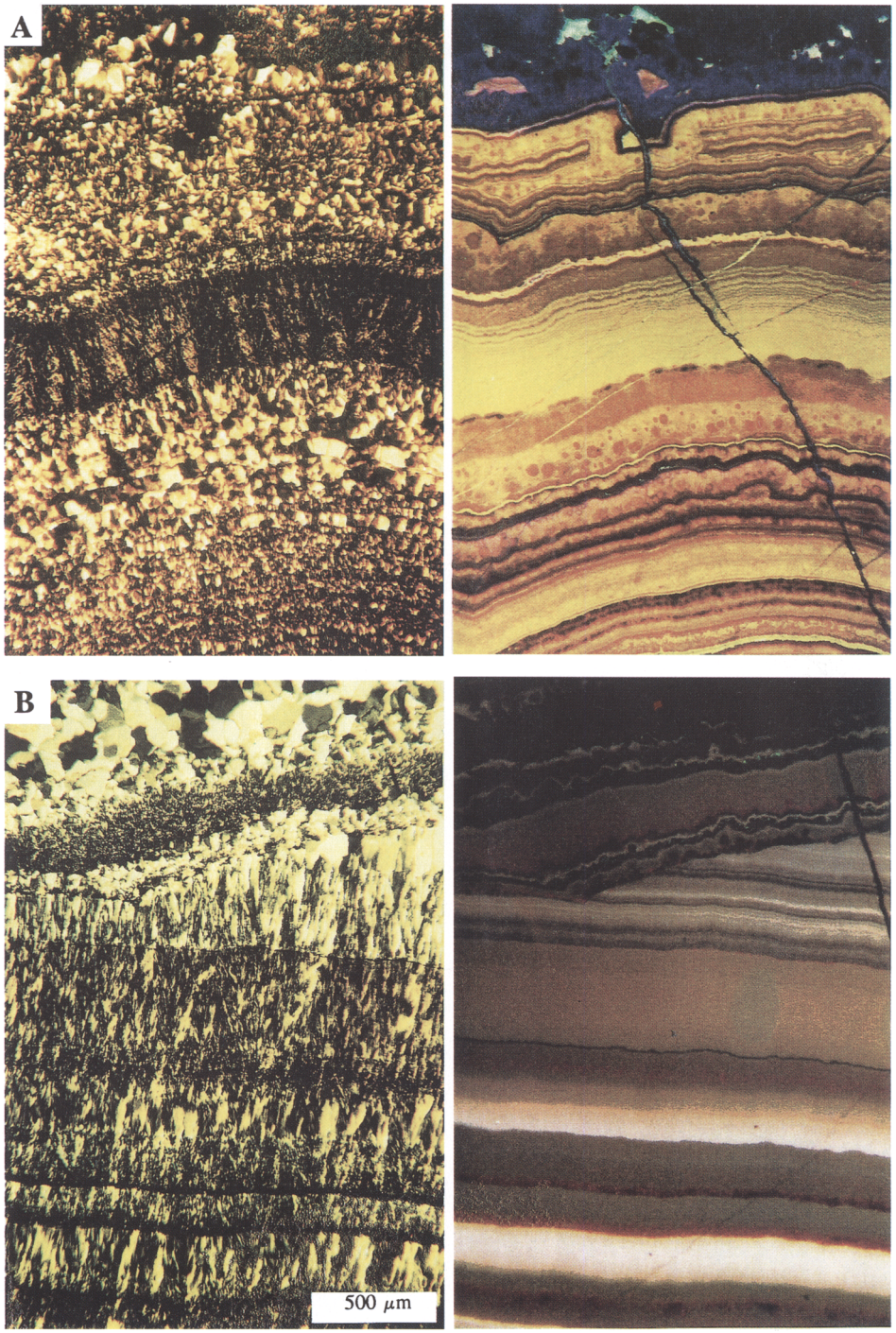

PLATE 2. Crossed polars/cathodoluminescence pairs of veinlike agates from acidic volcanics showing multicoloured cathodoluminescence zoning: (A) agate from Halsbach, Germany; (B) agate from Schlottwitz, Germany.

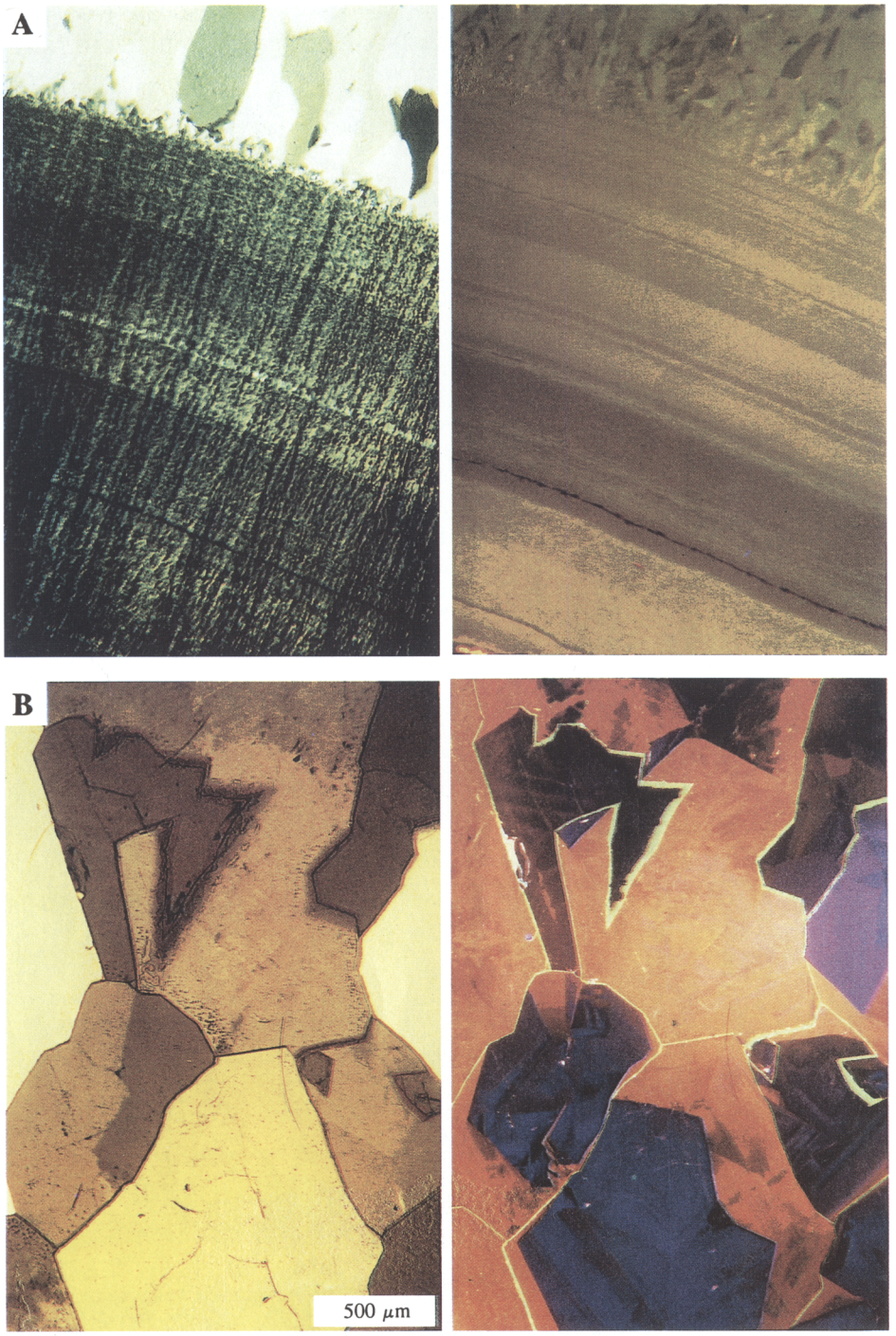

PLATE 3. Crossed polars/cathodoluminescence pairs of agates from basic volcanics: (A) agate from Idar-Oberstein (Germany) showing final brown cathodoluminescence after electron bombardement; (B) quartz within agate from Montrose (Scotland) exhibiting irregular cathodoluminescence features.

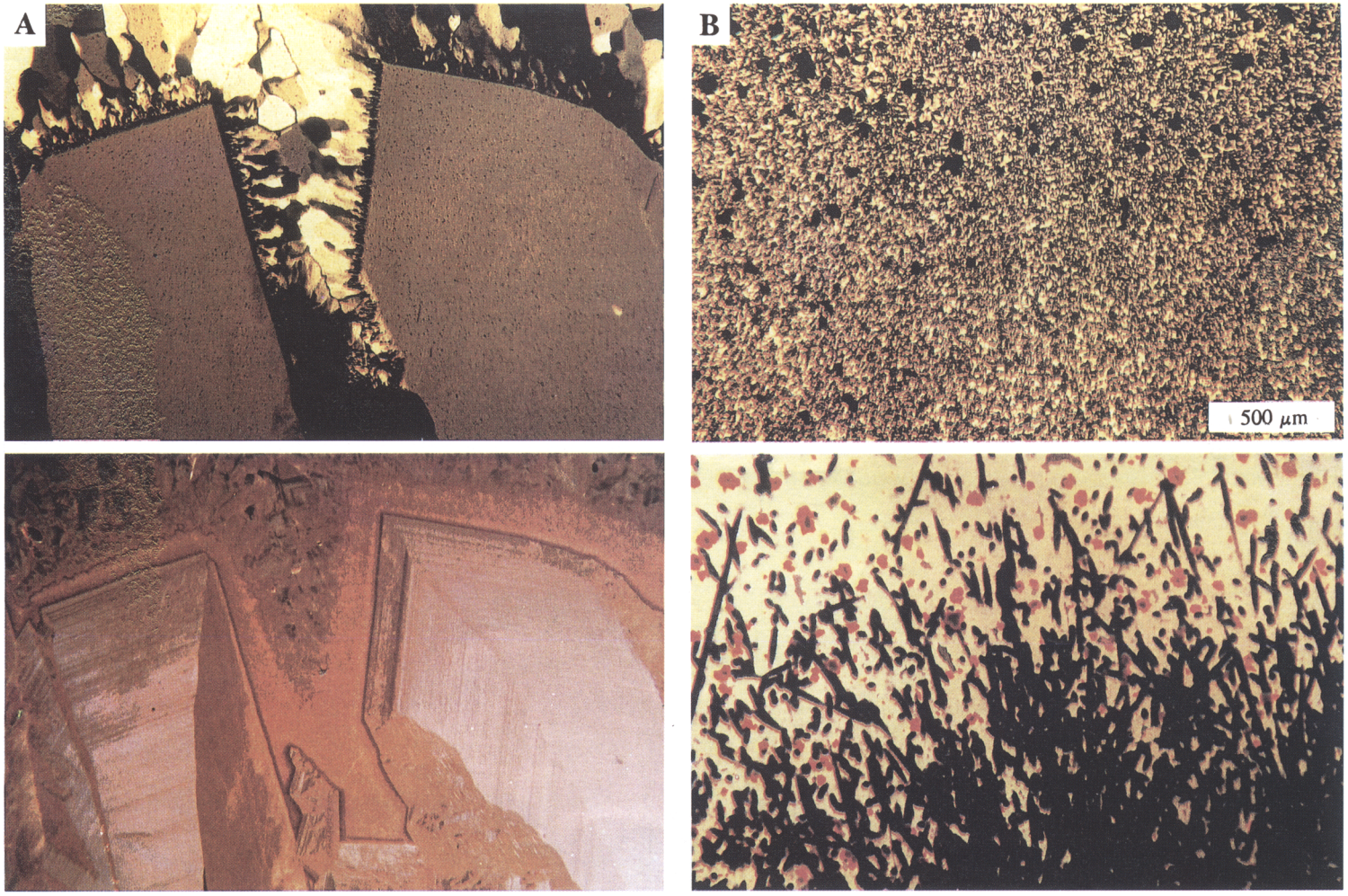

PLATE 4. Structural characteristics of agates and quartz incrustations revealed by cathodoluminescence: (A) quartz incrustation within agate from Gröppendorf, Germany; (B) cryptocrystalline silica in agate from Halsbach, Germany; in both figures cathodoluminescence reveals distinct zoning and internal structures remarkably differing from those visible under crossed polars.